X-band Rectangular to Square Waveguide Transition for Transmitarray Unit Cell Characterization

Muhammad Naeem Iqbal, Mohd Fairus Mohd Yusoff, Mohammad Kamal A Rahim,
Mohamad Rijal Hamid, Zaharah Johari
Advanced RF and Microwave Research Group, School of Electrical Engineering, Faculty of Engineering,
Universiti Teknologi Malaysia, (UTM), 81300 Skudai, Johor Bahru, Malaysia

***Abstract*-In this paper, a characterization setup for transmitarray unit cell analysis is designed in CST studio using rectangular to square waveguide transition for X-band applications. A wideband transmitarray unit cell is designed using split ring resonator and unit cell simulations show wide impedance matching bandwidth of 43.7%. In this simulation, the waveguide transition length is varied to reduce the reflection coefficient magnitudes below -20dB. Then, the square cross section area of waveguide is made variable and cutoff frequency variation over 4GHz is illustrated. Finally, the model for real time test setup is simulated along with the transmitarray unit cell and the results show high transmission magnitude of -0.23dB. This setup can also be used for other frequency selective surface unit cells characterization.**

I. INTRODUCTION

The transmitarray (TA) antennas belong to the family of high gain antennas having the advantage of low profile, no source blockage as in reflectarray antennas and the beam switching capabilities. The research work on transmitarray antennas started in in 1968 with the renowned HAPDAR design [1]. Subsequently, it has taken the form of lens antennas [2-13] due to its phase convergence and compensation capability. It also enhances the directivity of space-fed transmitarray by generating the pencil beam radiation pattern. Previously, the research work was focused mainly towards the transmitarray antenna designs using receiver-transmitter type configurations in which three layers were mostly used [11, 14-20]. The bottom layer in these configurations works as a receiver layer and the top most layer as the transmitter layer. However, the middle layer provides the isolation as well as phase delay required for phase compensation in each unit cell. Moreover, the complexity of complete transmitarray design can increase due to the involvement of vias and layer alignment issues. The involvement of active devices in the middle layer can also increase the causes of errors manifolds. Frequency selective surface (FSS)-based multilayer transmitarrays are being designed [6, 21-28] to reduce complexity, with high transmittance magnitude and can cover full 360^0 phase range.

Waveguide sets are required for characterization of FSS-based TA unit cell using a 2-port vector network analyzer. However, the waveguides available have rectangular and circular shapes which is not directly compatible with square TA unit cell. Due to this, we have designed rectangular to square waveguide transition.

In this research work, we will design the frequency selective surface-based transmitarrays unit cell. The simulation results of TA unit cell using rectangular to square waveguide transitions will be analyzed. The parametric analysis using waveguide transition length and square cross section area is performed. The E-field two-dimensional plots along the waveguide transition is illustrated. Lastly, s-parameter results before and after the placement of FSS layers will be analyzed.

II. UNIT CELL AND RECTANGULAR TO SQUARE WAVEGUIDE TRANSITION DESIGN

The unit cell design for frequency selective surface based transmitarray antenna is made at 10GHz. In this design, we have increased transmittance bandwidth by introducing a Split Ring Resonator (SRR) based TA unit cell. The complete dimensions of SRR unit cell are shown in Figure 1. The substrate used for TA unit cell design is FR4 with relative permittivity of 4.4 and thickness of 0.5mm. The thickness of Copper strip is 0.035um and strip width is 0.4mm for high transmittance magnitudes.

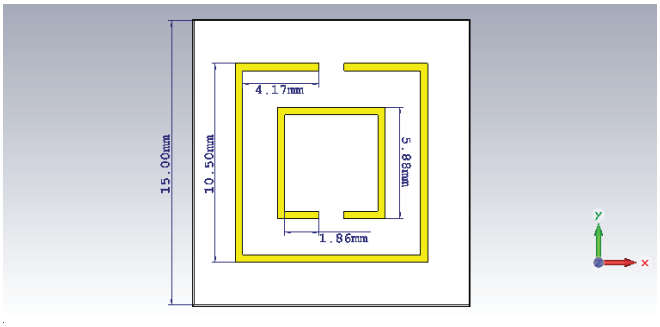

Figure 1. Split ring resonator-based TA unit cell Design at 10GHz

The rectangular waveguide standard WR90 specifications are used for simulations. For WR90 rectangular waveguide, the cutoff frequency is 6.7GHz. In order to match the cutoff frequency, the side length of square section of waveguide transition is selected to be 22.86mm. The material used for waveguide transition is Lossy Aluminum with high conductivity of 3.56 x 10^7 S/m. Top, bottom and side views of waveguide transition with the complete dimensions are shown in Figures 2(a), (b) and (c), respectively. The square section is matched with the standard WR90 rectangular waveguide section using CST loft technique.

978-1-7281-2396-7/19/$31.00 ©2019 IEEE

Authorized licensed use limited to: UNIVERSITY TEKNOLOGI MALAYSIA. Downloaded on April 29,2021 at 04:44:57 UTC from IEEE Xplore. Restrictions apply.

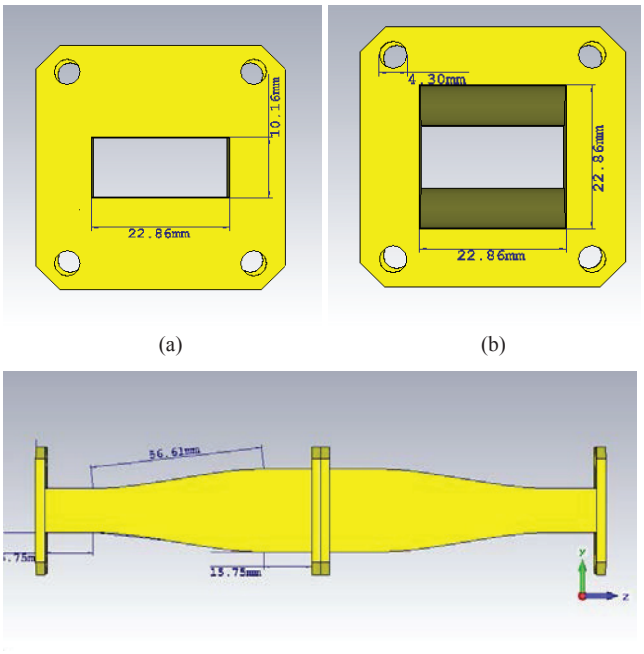

(a) (b)

(c)

Figure 2. (a) Rectangular waveguide section (b) Square waveguide section for unit cell (c) Side view for waveguide transition illustration

In order to match the square waveguide section with the unit cell dimensions, the square cross section area can be varied. By this way, the dimensions as well as cutoff frequency of the waveguide transition can be matched. Figure 3 shows the waveguide transition with reduced square side length of 15mm to match the unit cell dimensions at 10GHz. In this simulation, the square cross-sectional area is kept variable to see its effect on cutoff frequency.

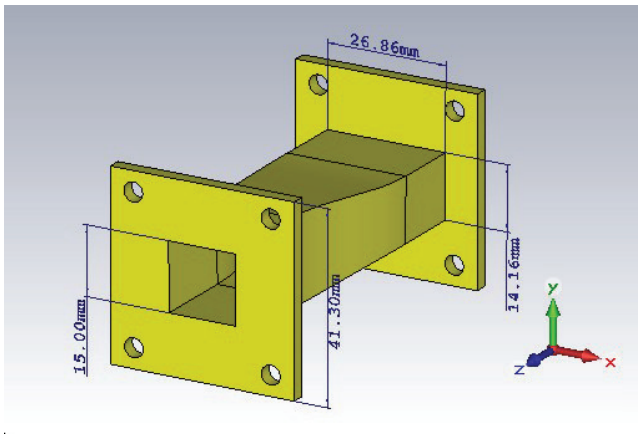

Figure 3. Variable square waveguide section for cutoff frequency variation

The cutoff frequency of WR90 rectangular waveguide is 6.7GHz with dimension "a" value of 22.86mm. For the final measurement setup, we will use the same side length "a" of 22.86mm as shown in Figure 4. This will match the cutoff frequency with the WR90 waveguide section. The SRR based TA unit cell as shown in Figure 1 is placed in between the two transitions.

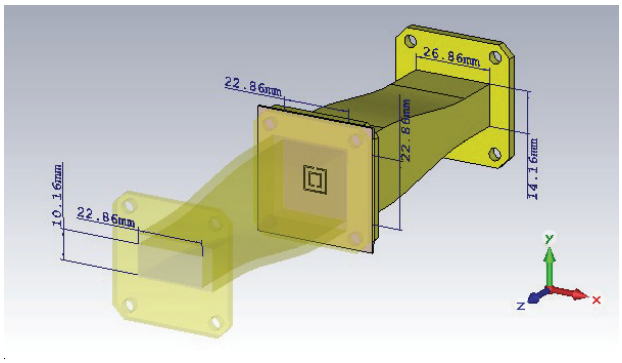

Figure 4. Waveguide transitions with the unit cell measurement setup

III. RESULTS

The s-parameter magnitude and phase plots for X-band (8-12GHz) are shown in Figures 5 and 6, respectively. The results show high S21 magnitude of -0.37dB, S11 magnitude below -20dB and wide impedance matching bandwidth of 43.7%.

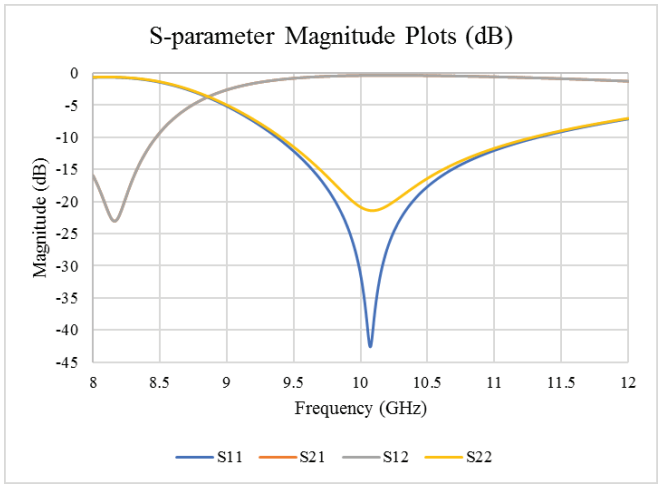

Figure 5. Transmittance magnitude of SRR unit cell

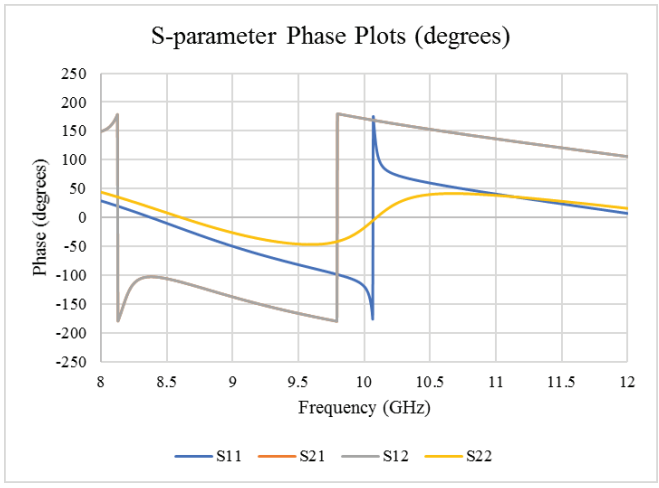

Figure 6. Transmittance phase of SRR unit cell

The effect of changing the waveguide transition length over the reflection and transmission magnitude is shown below in figure 7 and 8 below. By increasing the length of waveguide transition, we see that the transmission magnitude increases and the ripples in both the plots reduce to a

Authorized licensed use limited to: UNIVERSITY TEKNOLOGI MALAYSIA. Downloaded on April 29,2021 at 04:44:57 UTC from IEEE Xplore. Restrictions apply.

maximum value of 56.25mm, at which the all the S11 values are below -10dB.

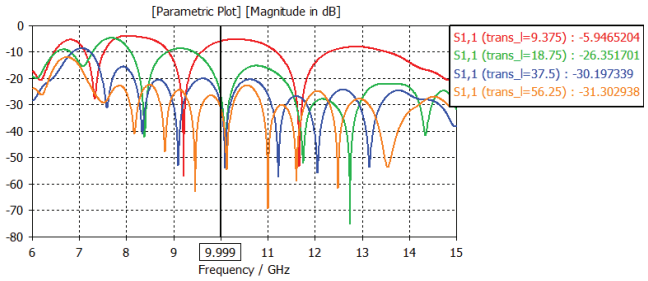

Figure 7. S11 Magnitude plots for varying transition lengths

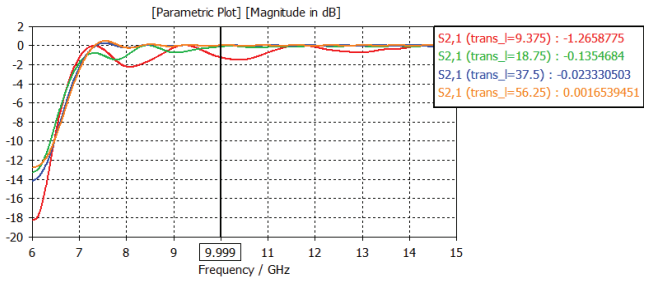

Figure 8. S21 Magnitude plots for varying transition lengths

The cutoff frequency variation can be seen with the square side length variation in the S21 and S11 magnitude plots in Figures 9 and 10, for the variable square section model shown in Figure 3. The cutoff frequencies for square waveguide side length values of 15, 17, 19 and 21mm are shifted to 7.34, 8.02, 8.93 and 10.14 GHz, respectively.

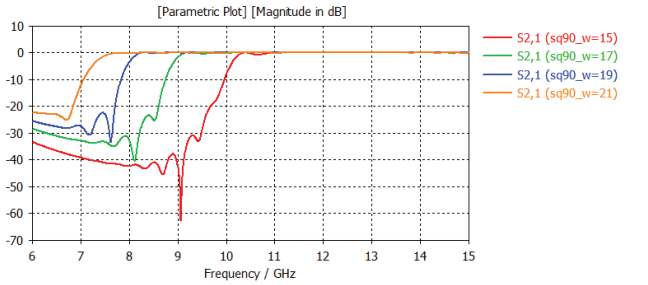

Figure 9. S21 magnitude plots for variable square waveguide section

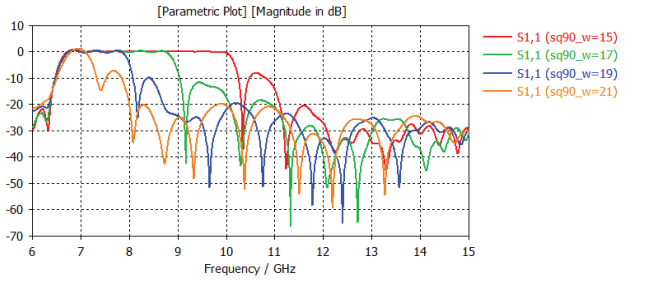

Figure 10. S11 magnitude plots for variable square waveguide section

The s-parameter magnitude and phase plots for the final measurement setup (Figure 4) are given in Figures 11 and 12. From the Figure 11, high transmission magnitude of -0.23dB and very low reflection magnitude of -26.44dB is obtained at center frequency of 10GHz. This illustrates the high transmittance of split ring resonator-based transmitarray unit cell.

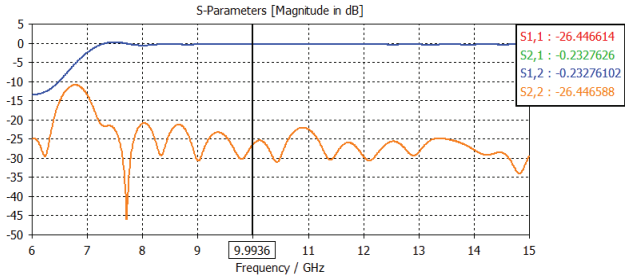

Figure 11. s-parameter magnitude plot of test setup

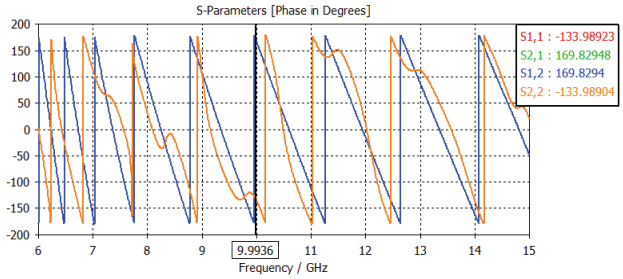

Figure 12. s-parameter phase plot of test setup

The E-field propagation along the waveguide transitions-based back-to-back setup with the SRR transmitarray unit cell is shown in Figure 13. The maximum E-field values can be seen at both the port ends. In the middle, the E-field is distributed with lower magnitudes due to larger waveguide cross-sectional area and unit-cell between two rectangular to square waveguide transitions.

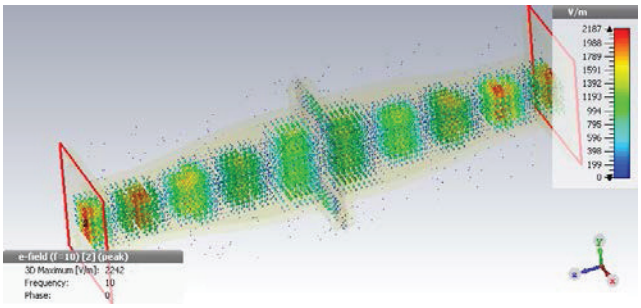

Figure 13. Two-dimensional E-field plot at 10.5GHz

IV. Conclusion

In this research, a wideband split ring resonator-based transmitarray unit cell is designed using CST studio at 10GHz. The unit cell has wide impedance bandwidth of 43.7% along with high transmission magnitude. The rectangular to square waveguide transition is designed for FSS unit cell characterization setup. The parametric simulations are performed with transition length variation to reduce the reflections magnitude below -20dB. The square waveguide cross section area is varied for cutoff frequency adjustment over 4 GHz frequency range. Complete test setup comprised of unit cell with the rectangular to square waveguide transition is simulated and high transmission magnitude of -0.23dB is obtained.

Authorized licensed use limited to: UNIVERSITY TEKNOLOGI MALAYSIA. Downloaded on April 29,2021 at 04:44:57 UTC from IEEE Xplore. Restrictions apply.

ACKNOWLEDGEMENTS

The authors would like to thank the Ministry of Higher Education (MOHE), Research Management Centre (RMC), School of Electrical Engineering, Universiti Teknologi Malaysia (UTM) for supporting the research work, under grant no. 14J22.

REFERENCES

[1] P. Kahrilas, "HAPDAR—An operational phased array radar," *Proceedings of the IEEE,* vol. 56, pp. 1967-1975, 1968.

[2] S. V. Hum and J. Perruisseau-Carrier, "Reconfigurable reflectarrays and array lenses for dynamic antenna beam control: A review," *IEEE Transactions on Antennas and Propagation,* vol. 62, pp. 183-198, 2014.

[3] M. Li, M. A. Al-Joumayly, and N. Behdad, "Broadband true-time-delay microwave lenses based on miniaturized element frequency selective surfaces," *IEEE Transactions on Antennas and Propagation,* vol. 61, pp. 1166-1179, 2013.

[4] M. Li and N. Behdad, "Ultra-wideband, true-time-delay, metamaterial-based microwave lenses," in *Proceedings of the 2012 IEEE International Symposium on Antennas and Propagation*, 2012, pp. 1-2.

[5] Y. Zhang, R. Mittra, and W. Hong, "On the synthesis of a flat lens using a wideband low-reflection gradient-index metamaterial," *Journal of Electromagnetic Waves and Applications,* vol. 25, pp. 2178-2187, 2011.

[6] M. A. Al-Joumayly and N. Behdad, "Wideband planar microwave lenses using sub-wavelength spatial phase shifters," *IEEE Transactions on Antennas and Propagation,* vol. 59, pp. 4542-4552, 2011.

[7] S. Kamada, N. Michishita, and Y. Yamada, "Metamaterial lens antenna using dielectric resonators for wide angle beam scanning," in *2010 IEEE Antennas and Propagation Society International Symposium*, 2010, pp. 1-4.

[8] Q. Cheng, H. F. Ma, and T. J. Cui, "Broadband planar Luneburg lens based on complementary metamaterials," *Applied Physics Letters,* vol. 95, p. 181901, 2009.

[9] C.-C. Cheng, B. Lakshminarayanan, and A. Abbaspour-Tamijani, "A programmable lens-array antenna with monolithically integrated MEMS switches," *IEEE Transactions on Microwave Theory and Techniques,* vol. 57, pp. 1874-1884, 2009.

[10] S. Datthanasombat, A. Prata, L. Arnaro, J. Harrell, S. Spitz, and J. Perret, "Layered lens antennas," in *IEEE Antennas and Propagation Society International Symposium. 2001 Digest. Held in conjunction with: USNC/URSI National Radio Science Meeting (Cat. No. 01CH37229)*, 2001, pp. 777-780.

[11] D. Pozar, "Flat lens antenna concept using aperture coupled microstrip patches," *Electronics Letters,* vol. 32, pp. 2109-2111, 1996.

[12] D. McGrath, "Planar three-dimensional constrained lenses," *IEEE Transactions on Antennas and Propagation,* vol. 34, pp. 46-50, 1986.

[13] R. Milne, "Dipole array lens antenna," *IEEE Transactions on Antennas and Propagation,* vol. 30, pp. 704-712, 1982.

[14] A. Clemente, L. Dussopt, R. Sauleau, P. Potier, and P. Pouliguen, "Wideband 400-element electronically reconfigurable transmitarray in X band," *IEEE Transactions on Antennas and Propagation,* vol. 61, pp. 5017-5027, 2013.

[15] A. Clemente, L. Dussopt, R. Sauleau, P. Potier, and P. Pouliguen, "Design of a reconfigurable transmit-array at X-band frequencies," in *2012 15 International Symposium on Antenna Technology and Applied Electromagnetics*, 2012, pp. 1-4.

[16] H. Kaouach, L. Dussopt, J. Lanteri, T. Koleck, and R. Sauleau, "Wideband low-loss linear and circular polarization transmit-arrays in V-band," *IEEE Transactions on Antennas and Propagation,* vol. 59, pp. 2513-2523, 2011.

[17] P. Padilla, A. Muñoz-Acevedo, M. Sierra-Castañer, and M. Sierra-Pérez, "Electronically reconfigurable transmitarray at Ku band for microwave applications," *IEEE Transactions on Antennas and Propagation,* vol. 58, pp. 2571-2579, 2010.

[18] J. Y. Lau and S. V. Hum, "A low-cost reconfigurable transmitarray element," in *2009 IEEE Antennas and Propagation Society International Symposium*, 2009, pp. 1-4.

[19] P. Padilla de la Torre and M. Sierra-Castañer, "Design and prototype of a 12-GHz transmit-array," *Microwave and Optical Technology Letters,* vol. 49, pp. 3020-3026, 2007.

[20] H. J. Song and M. E. Bialkowski, "Transmit array of transistor amplifiers illuminated by a patch array in the reactive near-field region," *IEEE Transactions on Microwave Theory and Techniques,* vol. 49, pp. 470-475, 2001.

[21] S. H. R. Tuloti, P. Rezaei, and F. T. Hamedani, "High-Efficient Wideband Transmitarray Antenna," *IEEE Antennas and Wireless Propagation Letters,* vol. 17, pp. 817-820, 2018.

[22] C.-Y. Hsu, L.-T. Hwang, T.-S. Horng, S.-M. Wang, F.-S. Chang, and C. N. Dorny, "Transmitarray Design with Enhanced Aperture Efficiency Using Small Frequency Selective Surface Cells and Discrete Jones Matrix Analysis," *IEEE Transactions on Antennas and Propagation,* 2018.

[23] R. Y. Wu, Y. B. Li, W. Wu, C. B. Shi, and T. J. Cui, "High-gain dual-band transmitarray," *IEEE Transactions on Antennas and Propagation,* vol. 65, pp. 3481-3488, 2017.

[24] C. Tian, Y.-C. Jiao, G. Zhao, and H. Wang, "A wideband transmitarray using triple-layer elements combined with cross slots and double square rings," *IEEE Antennas and Wireless Propagation Letters,* vol. 16, pp. 1561-1564, 2017.

[25] C. Tian, Y.-C. Jiao, and G. Zhao, "Circularly polarized transmitarray antenna using low-profile dual-linearly polarized elements," *IEEE Antennas and Wireless Propagation Letters,* vol. 16, pp. 465-468, 2017.

[26] C. Fan, W. Che, W. Yang, and W. Feng, "A polarization-rotation AMC-based low-profile transmitarray antenna," in *Microwave Conference (APMC), 2016 Asia-Pacific*, 2016, pp. 1-4.

[27] A. H. Abdelrahman, A. Z. Elsherbeni, and F. Yang, "Transmission phase limit of multilayer frequency-selective surfaces for transmitarray designs," *IEEE Transactions on Antennas and Propagation,* vol. 62, pp. 690-697, 2014.

[28] C. G. Ryan, M. R. Chaharmir, J. Shaker, J. R. Bray, Y. M. Antar, and A. Ittipiboon, "A wideband transmitarray using dual-resonant double square rings," *IEEE Transactions on Antennas and Propagation,* vol. 58, pp. 1486-1493, 2010.

Authorized licensed use limited to: UNIVERSITY TEKNOLOGI MALAYSIA. Downloaded on April 29,2021 at 04:44:57 UTC from IEEE Xplore. Restrictions apply.